

Wind/jet Formation in T Tauri Stars: Theory versus UV Observations

Ana I Gómez de Castro¹, Eva Verdugo², Constantino Ferro-Fontán³

Abstract.

Observations of the base of protostellar jet carried out with HST-STIS are presented. The Si III] and CIII] profiles are analyzed for 6 T Tauri stars (TTSs). It is found that the line emission is produced in the stellar atmosphere and in the base of the optical jet. The presence of a low density ($10^4 - 10^5 \text{ cm}^{-3}$) envelope is detected. High densities ($\sim 10^{10} \text{ cm}^{-3}$) of the line formation region are confirmed for RU Lup.

These results are compared with the theoretical predictions of magneto-centrifugal disk winds. It is shown that densities above 10^8 cm^{-3} cannot be produced by disk winds. The main spectral signature of disk winds is shown to be the presence of asymmetric absorption components in the blue-wing of strong resonance lines. The strength of the components depends on the inclination and on the accretion rate.

1. Introduction

Outflow is ubiquitous during star formation: it is observed from the very early phases (class 0 sources) to the late stages of the pre-main sequence evolution. Bipolar flows are widely assumed to be powered by the gravitational energy released during the accretion process and the magnetic field is often hypothesized as the physical stress which efficiently channels the gravitational energy into the mechanical outflow energy (see e.g. Shu et al 2000, Koenigl & Pudritz 2000 for recent reviews). Determining the precise physical mechanism that connects accretion to outflow is one of the key issues in star formation since this regulates the accretion rate and the evolution during the pre-main sequence phase. Moreover, it seems likely that the same physics applies to other astrophysical systems such as QSOs, AGNs or microquasars.

The T Tauri phase is probably the most interesting phase to study the mechanism driving the outflow in pre-main sequence stars. At this stage bipolar flows, often detected as optical jets, are still active but the central engine can be observed at optical and ultraviolet wavelengths allowing a detailed spectroscopic diagnosis.

¹Instituto de Astronomía y Geodesia (CSIC-UCM), Universidad Complutense de Madrid, Spain

²ISO Data Center, Spain

³Consejo Superior de Investigaciones Científicas y Técnicas (CONICET-Argentina), Universidad de Buenos Aires, Argentina

To obtain information about the physics of jet formation it is necessary to go below scales of ~ 10 AU. Hirth et al. (1997) have shown that the jet streamlines diverge with the distance from the source giving rise to a drop in density. If the density of the jet increases towards the source, the electron density at the base of the jet could be even higher than 10^6 cm^{-3} traced by the $[\text{O I}]_{6300}$ optical line. The UV semiforbidden lines are optimal tracers at these very high densities. The $\text{C III]} (2s \ ^2\text{S}_1-2s2p \ ^3\text{P}_1)$ and $\text{Si III]} (3s \ ^2\text{S}_1-3s3p \ ^3\text{P}_1)$ UV intercombination lines are strong in the spectrum of the TTSs (see e.g. Gómez de Castro 1997 for a recent review). The ratio $I(\text{Si III]})/I(\text{C III]})$ is density sensitive and it is often used to estimate electron densities in late-type stellar atmospheres within the range $10^8 \leq N_e \leq 10^{13} \text{ cm}^{-3}$ (see Brown et al. 1984 for its application to T Tau). Recently, it has been shown that these lines could also be formed in accretion shocks (shocks where the kinetic energy from the material falling onto the stellar surface is released); the C III] and Si III] lines are expected then, to be formed before the shock front where the infalling gas is ionized by the X-rays radiation produced in the hot ($T \sim 10^6$ K) post-shock region (Lamzin 1998; Gómez de Castro & Lamzin 1999). Moreover, the C III] and Si III] lines could also be excited in shocks at the base of the jet where the wind is collimated into a narrow beam of gas. In summary, these lines are an extraordinary diagnosis tool to study the major physical processes in the hot dense circumstellar environment around the TTSs. An additional advantage of these tracers is that they are accompanied by a nearby forbidden component and the ratios between the forbidden and the intercombination components of the $\text{C III]}_{1907,1909}$ and $\text{Si III]}_{1883,1892}$ multiplets are sensitive to electron densities in the range $N_e \simeq 10^3 - 10^6 \text{ cm}^{-3}$ (Keenan et al. 1992). Therefore a high resolution UV spectrum in the 1880-1910 Å spectral range provides direct diagnosis on electron densities over nearly 10 orders of magnitude!. This is an ideal tool for the study of the TTSs environment where many physical components are expected to be present and cannot be resolved spatially.

In this work, we present the results of an observational program run with the HST/STIS to obtain high resolution profiles of the $\text{C III]}_{1907,1909}$ and $\text{Si III]}_{1883,1892}$ lines in 6 TTSs. We show that the C III] and Si III] emission originates in the stellar atmosphere and also in the unresolved optical jet. A low density envelope contributing to the line emission has been found around RU Lup and T Tau. These observations are compared with the predictions of the centrifugally driven hydromagnetic disk winds.

2. HST/STIS observations

The observing program (GO-8628) was run between September 2000 and April 2001. The STIS G230M grating used has an average dispersion of 14 km/s (or 0.09 Å) per pixel. Some relevant properties of the targets observed are summarized in Table 1. Optical jets have been resolved in three of the six sources: T Tau, RW Aur and RU Lup (Hirth et al 1997, Takami et al 2001). Blueshifted forbidden line emission (FLE) has been detected in DE Tau and RY Tau by Hartigan et al (1995) and Hamman and Persson (1992) respectively. AK Sco is an spectroscopic binary and was observed at phase 0.2439 close after the secondary eclipse (see Andersen et al 1989).

Table 1. Properties of the observed TTSs

Star	V_r Jet ([OI]) (km/s)	$V \sin i$ (km/s)	Multiplicity
DE Tau	-100	10	Single
RU Lup	-120		Single
RY Tau	-80	52.2	Binary
T Tau	-115	20.1	Multiple
RW Aur	-167, 122	17.2	Multiple
AK Sco		19.0	Spec. Bin. (a = 0.1AU)

The Si III] and C III] profiles are displayed in Fig 1. The velocity of the optical jet, as derived from the [OI]₆₃₀₀ profile, is marked in the plot. Notice that the Si III],C III] counterparts of the optical jet are clearly observed in most sources. This is not surprising. A quick look at the UV spectra of protostellar jets (see e.g. Gómez de Castro & Robles, 1999) shows that the C III] line is very strong in the spectra. The main difference is that in the TTSs the Si III] line is often as strong, or even stronger, than the C III] line. A quick look at the profiles also shows that:

1. There is always an emission peak centered at the stellar velocity which is most likely associated with atmospheric emission.
2. The forbidden component of the C III] at $\lambda 1907\text{\AA}$ is observed in RU Lup and in T Tau over a broad velocity range. This indicates the presence of low density plasma ($N_e = 10^4 - 10^5 \text{ cm}^{-3}$) around these two stars. This low density plasma has two basic components: one at rest with respect to the star and another at the jet velocity. Therefore, it has similar kinematical properties to the optical tracers in this density range. This indicates that a fraction of the C III] (and Si III]) emission is produced in a low density jet. The low density zero-velocity emission is most probably produced in a low density gas envelope around the star photoionized by the strong X-rays flux.
3. The forbidden component of the C III] at $\lambda 1907\text{\AA}$ is not observed in DE Tau, RW Aur, AK Sco and RY Tau. This provides lower limits to the jet density that range from 10^5 cm^{-3} in DE Tau to 10^6 cm^{-3} in RY Tau for which the $C_{III]1907}/C_{III]1909}$ reaches the saturation limit.

The most intriguing source is RY Tau. It is clear from the observations that the strength of the stellar and jet components are comparable in the Si III] and the C III] profiles. Also some redshifted components are observed in the Si III] profile. These data confirm the presence of a high density outflow from RY Tau (Gómez de Castro & Verdugo, 2001) but leave still open a precise determination of the outflow density since there is not information available for a precise determination of the temperature of the emitting region.

The presence of a high density outflow is definitely confirmed for RU Lup. As shown in Fig. 2 the red wing of the O III]₁₆₆₆ line is absorbed for velocities

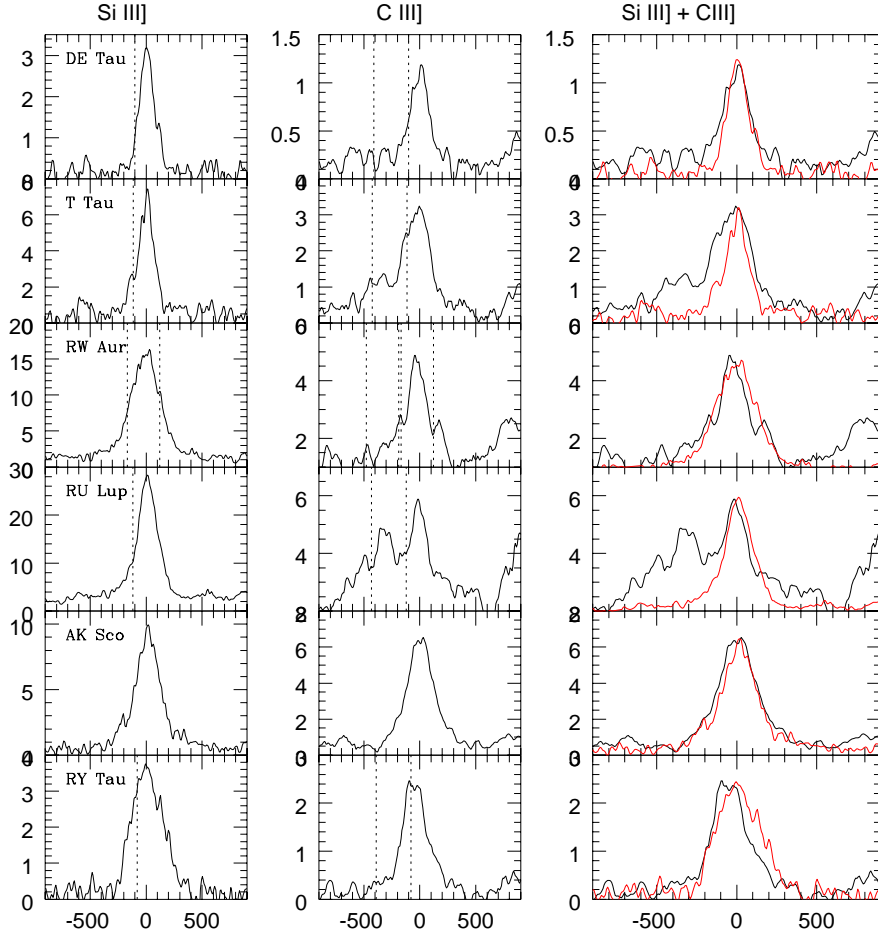


Figure 1. Si III] and C III] profiles (flux versus radial velocity) are plotted for the program stars in the left and central panels respectively. In the right panels, the Si III] profile (red) is scaled to the C III] flux (black) and overplotted for comparison. The velocity of the blueshifted forbidden line emission from the optical jets is marked with dashed lines in the left and central panels. Notice that in T Tau and RU Lup the forbidden component of the C III] is detected pointing out that most of the emission is produced in a low density envelope (see the text). The radial velocity is given in Km/s with respect to the star and the flux in units of 10^{-14} erg cm $^{-2}$ s $^{-1}$ Å $^{-1}$.

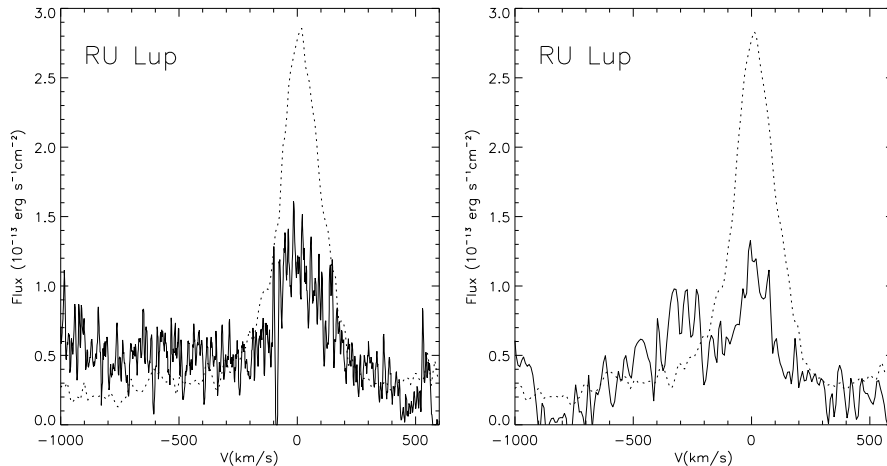


Figure 2. O III], Si III] and C III] profiles of RU Lup. The O III] and C III] are multiplied by a factor of 3 in order to be compared with the Si III] profile (dashed line in both panels)

higher the 100 km/s. This line has a critical density of $N_{\text{cr}} = 3.4 \times 10^{10} \text{ cm}^{-3}$ for $T_e = 15000 - 20000 \text{ K}$ that is significantly smaller than the critical density of the C III] and the Si III]. Therefore, absorption by warm dense gas is most probably responsible for the asymmetric profile. This profile is also observed in the Mg II (uv1) lines and in the HeII Balmer α line. It is however, puzzling that the Si III] emission extends further to the blue than the O III] reaching the optical jet velocity, as well as the detection of C III] emission from both the forbidden and the semiforbidden lines.

3. MHD disk wind models

Centrifugally driven disk winds are expected to remove a significant fraction of the angular momentum of the accretion disk from the early stages of star formation until the classical TTS (cTTS) phase (see e.g. Koenigl & Pudritz, 2000). The optical jets produced during this phase are often barely resolved, and they are detected mainly by their [OI] $_{6300}$ emission. This emission is thought to be generated as the radiative output of a shock wave formed in the disk winds (Gómez de Castro & Pudritz, 1993). The STIS observations of the Si III] and C III] lines point out there is also significant UV emission from this region.

Shock waves can be easily generated in centrifugally driven MHD disk winds. The shock is produced if the magnetic tension from the toroidal component is so strong as to recollimate (pinch) the flow back to the axis at super-alfvénic speeds. In this sense, the magnetic field acts as a nozzle which efficiently collimates and accelerates the outflow. This physics applies to all kind of centrifugally driven MHD winds independently of the source of the wind (star, disk, magnetosphere; see e.g. Pelletier & Pudritz 1993, Contopoulos & Lovelace 1994, Vlahakis & Tsiganos 1998). A general property of shocks produced in MHD

flows is that the amount of energy that goes into the heat channel depends strongly on the plasma β^1 which measures the relevance of magnetic fields in the plasma dissipative processes. This value is very difficult to determine from the observations, and thus there is a broad range of thermal properties (for the shock wave) which can be accommodated within the available theoretical models. Therefore, no significant constraints to wind/jet models can be derived from them. This is not so for other parameters of the shock wave such as density, location and characteristic size.

We have studied the MHD equations that describe the wind-disk connection to be able to track the properties of the wind from the disk to the shock, to derive the density and velocity law of the wind, and to determine the location and characteristics of the refocussing point. The equations employed in the theory are the usual ones of resistive hydromagnetics, with a magnetic diffusivity enhanced by turbulent processes, following the exhaustive discussion of the exact equations, including heating and radiation processes, made by Ferreira & Pelletier (1993, 1995) and Ferreira (1997). Important questions answered by the model concern accretion flow, toroidal field generation by differential rotation of the layered material, magnetic buoyancy and compression stresses. When the magnetic thrust is that appropriate to lift up a vertical ejection flow, the edge of the boundary layer is topped with a sonic throat, beyond which expands a supersonic, ideal MHD jet (see Ferro-Fontán & Gómez de Castro in preparation).

The feasibility of magnetic levitation and henceforth, wind formation depends critically on the parameter μ that measures the strength of the Lorentz forces relative to tidal forces. The range of permitted values is very small; e.g. for a disk profile with $\epsilon = 0.01$, where $\epsilon = h/r$ is the ratio between the height over the disk and the radial distance, μ must be between 0.35 and 0.85 to allow the formation of a disk wind. The space of solutions can be separated into two quite different classes according to the value of μ . Low efficiency solutions, typically $\mu \lesssim 0.64$, have been recently examined by Cabrit et al (1999). They display a characteristic density change, from horizontal to vertical stratification, at a colatitude of the order of $\frac{1}{2}\theta_A$. These solutions are magnetically dominated in the sense that most of the angular momentum flux is carried out by the Poynting vector. The radial expansion factor of these jets is large and they recollimate very far from the disk plane. On the contrary, high- μ solutions have a monotonic behaviour: the density decreases, without any intermediate enhancement, as one approaches the rotation axis at constant z . However we note that, in *both* types of solution, the jet terminates in a central *hollow* cone. The opening angle of this cone is very small for low- μ solutions so, in most cases, the cone goes unnoticed, but for high μ values, it is a sizable fraction of the Alfvén angle θ_A . Figure 3 illustrates the evolution of the density profiles in the transition interval from $\mu = 0.64$ to 0.070.

Our analytical models are r -self similar and therefore they are best suited to study the dynamics of disk winds close to the disk plane. The models are expected to be unrealistic close to the disk axis; however, recent numerical simulations carried out by Krasnopolsky et al (1999) also show the presence of a density enhancement close to the axis for small values of μ . In summary, disk

¹ β is the ratio between the magnetic and thermal pressures

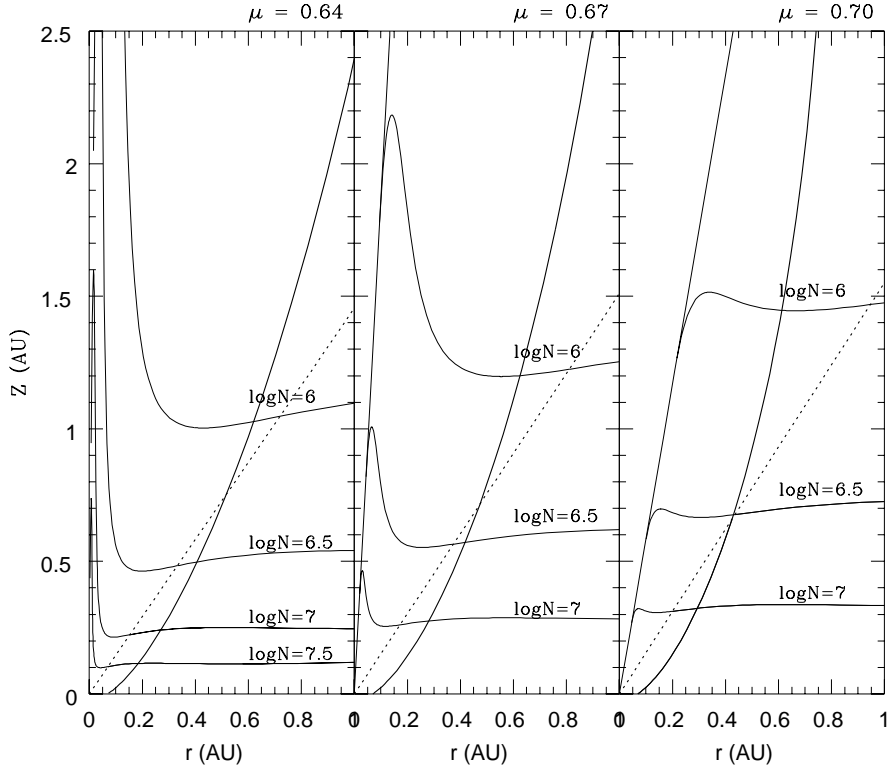


Figure 3. Structure of the disk wind depending on the parameter μ for $\epsilon = 0.03$. The thick line represents the trajectory of the wind departing from the inner edge of the disk. As the model is self-similar trajectories departing from other radii are similar. Notice that the refocussing (magnetic pinching) occurs at scales much larger than 2 AU. The dotted line represent the Mach-Alfvén cone (colatitude = θ_A). Finally the continuous lines are isodensity contours which are labelled in units of $\log N$ where N is the particle density in cm^{-3} . Notice that there is a hollow cone inside the disk wind which becomes clearly apparent as the value of μ increases (see the text). Notice also that the wind changes from horizontal to vertical density stratification at a colatitude which corresponds with $\frac{\theta_A}{2}$ for small values of μ .

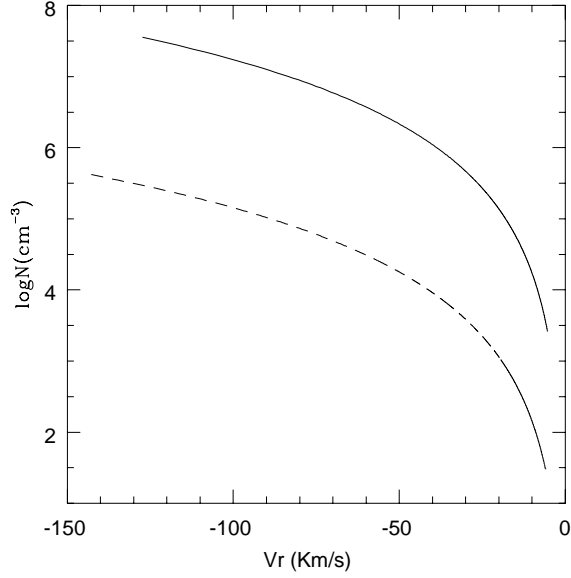


Figure 4. Density versus radial velocity of the disk wind material for inclinations $i = 75^\circ$ (continuous line) and $i = 45^\circ$ (dashed line); notice that $i = 90^\circ$ for an edge on disk. $\mu=0.70$

winds are expected to be latitude dependent, e.g. the wind absorbing gas column depends on the inclination of the line of sight with respect to the star. In principle, the column is maximum close to the disk plane ($i \sim 80^\circ$) and decreases as the inclination becomes smaller. Then, depending on μ , two distinct regimes are possible. For small μ 's, the flow density is expected to increase again as i approaches 0° . For high μ 's the density decreases steadily. This behaviour is described in more detail in Fig. 4 where the gas density is represented as a function of the radial velocity of the disk wind projected onto the line of sight. Also notice, that the largest absorption column is at the inner border of the wind where the highest velocities are achieved. Therefore, the spectral signature of cool disk winds is the presence of asymmetric absorption components in the bluewing of strong resonance lines.

4. Summary

In summary, disk winds are not very dense. At the base of the wind the density is $\sim 10^8 \text{ cm}^{-3}$ and the opening of the magnetic field lines caused by the centrifugal force, causes this density to drop by two orders of magnitude within 1.5 AUs of the star. Therefore it is very difficult to achieve densities above 10^6 in these outflows; these densities agree with those observed in optical jets. Moreover, the model does not impose severe constraints on the gas temperature whenever it is $\leq 10^4 \text{ K}$, therefore the material could be heated by magnetic waves, ambipolar diffusion or the ambient X-rays radiation up to these values (especially close to the star) without significantly modifying the dynamics.

It seems however clear, that there are two winds acting at least, in RU Lup. There is certainly an outflow associated with the optical jet and the rather low density ($\sim 10^4 \text{ cm}^{-3}$) gas. However, the presence of a dense wind is required to explain the peculiar profile of the O III], Mg II (uv1) and HeII Balmer α lines. The connection between these two outflows is still unclear.

Acknowledgments. This research has been partly financed by the Ministry of Science and Technology of Spain through the research grant AYA2000-966.

References

- Andersen, J., Lindgren, H., Hazen, M.L., Mayor, M. 1989, A&A, 219,142
Brown, A., & Ferraz, M.C. de M., & Jordan, C. 1984, MNRAS, 207, 831.
Cabrit, S., Ferreira, J., Raga, A.C. 1999, A&A, 343, L61
Contopoulos, J., & Lovelace, R.V.E. 1994, ApJ, 429, 139.
Ferreira, J. 1997, A&A, 319, 340
Ferreira, J. & Pelletier, G. 1993, A&A, 276, 625
Ferreira, J. & Pelletier, G. 1995, A&A, 295, 807
Ferro-Fontán & Gómez de Castro, A.I. in preparation
Gómez de Castro, A.I. 1997, in *Ultraviolet Astrophysics, Beyond the IUE Final Archive*, Sevilla, Spain. Eds. Wamsteker, W., & González-Riestra, R. ESA-SP 413, p. 59.
Gómez de Castro, A.I. & Pudritz, R.E. 1993, ApJ, 400, 748
Gómez de Castro, A.I. & Robles, A. 1999, *INES Access Guide to Herbig-Haro objects observed with IUE*, ESA-SP 1237. ESA Pub., Noordwijk (The Neetherlands).
Gómez de Castro, A.I. & Lamzin, S.A., 1999, MNRAS, 304, L41
Gómez de Castro, A.I. & Verdugo, E. 2001, ApJ, 548, 976
Hamman, F. & Persson, S.E. 1992, ApJSup Ser, 82, 247
Hartigan, P., & Edwards, S., & Ghandour, L. 1995, ApJ, 452, 736
Hirth, G.A., Mundt, R., Solf, J. 1997, A&ASS, 126, 437
Keenan, F.P., Feibelman, W.A., Berrington, K.A. 1992, ApJ, 389, 443
Koenigl, A. & Pudritz, R.E. 2000, in *Protostars and Planets IV*, Univ. of Arizona Press, p. 759

- Krasnopolsky, R., Li, Z-Y, Blandford, R. 1999, ApJ, 526 631
- Lamzin, S.A. 1998, Astron. Rep., 42, 322
- Pelletier, G. & Pudritz, R.E. 1992, ApJ, 394, 117.
- Shu, F., & Najita, J.R., & Shang, H., & Li, Z.-Y. 1999, Protostars and Planets IV, Univ. of Arizona Press, p.789
- Takami, M., Bailey, J., Gledhill, A., Chrysostomou, A., Hough, J.H. 2001, MNRAS, 323, 177
- Vlahakis, N., & Tsinganos, K. 1998, MNRAS, 298, 777.